Possible Superconductivity for Layered Metal Boride Carbide Compounds MB_2C_2 (M = Alkali, Alkaline-Earth or Rare-Earth Metals)

Wataru Hayami,[1*] Xavier Rocquefelte,[2] and Jean-François Halet[2,3]*

[1]Research Center for Materials Nanoarchitectonics, National Institute for Materials Science, Namiki 1-1, Tsukuba, Ibaraki 305-0044, Japan

[2]Univ Rennes, CNRS, Ecole Nationale Supérieure de Chimie de Rennes (ENSCR), Institut des Sciences Chimiques de Rennes (ISCR), UMR 6226, F-35000 Rennes, France

[3]CNRS–Saint-Gobain–NIMS, IRL 3629, Laboratory for Innovative Key Materials and Structures (LINK), National Institute for Materials Science (NIMS), Tsukuba 305-0044, Japan

Inorg. Chem. 2024, 63, 20975−20983

https://doi.org/10.1021/acs.inorgchem.4c02221

* Corresponding authors. E-mail: hayami.wataru@nims.go.jp (W.H.), Jean-Francois.Halet@univ-rennes.fr (J.-F. H.)

ABSTRACT

The possible emergence of superconductivity in layered metal boride carbide compounds MB_2C_2 (M = Sc, Y, Be, Ca) was investigated using density functional theory calculations upon the topology of a boron–carbon network and the nature of the metal. ScB_2C_2 and YB_2C_2 show metallic and superconductive properties with low critical temperatures (T_cs). The semi-conducting BeB_2C_2 compound may show superconductivity upon carrier doping with a high T_c of 47.8 K by hole doping – comparable to the structurally related MgB_2 superconductor – but with a low T_c by electron doping. In contrast, the semi-conducting CaB_2C_2 compound is predicted to be a superconductor by hole and electron doping but with low T_cs. These differences arise from the spatial distribution of electrons at the Fermi level. For compounds with low T_cs, electrons at the Fermi level are localized primarily on B and C π states perpendicular to the BC layers, experiencing minimal influence from atomic oscillations and resulting in weak electron–phonon interactions. Conversely, for a high T_c, electrons are found in σ-bonding states, leading to strong electron–phonon interactions. Electrons at the Fermi level in boron–carbon σ-bonding states seem to be a prerequisite to expect high T_c superconductivity in this kind of compound.

1. INTRODUCTION

With the recent advent of high-pressure superconducting metal hydrides,[1–3] exploring new superconductors with a high critical temperature (T_c) continues to be one of the main topics in the fields of materials science and condensed matter physics. It is generally accepted that, in the case of conventional Bardeen−Cooper−Schrieffer phonon-mediated superconductors, T_c strongly depends upon a large density of states (DOS) at the Fermi energy, strong electron−phonon coupling, and high-frequency phonons.[4] This has been shown for compounds consisting of nonmagnetic metals and light elements, such as alkali, alkaline-earth, and nonmagnetic and magnetic transition-metal borides and carbides, as well as quaternary rare-earth-metal–transition-metal boride carbides, for instance.[5–17] Among these compounds, the well-known magnesium diboride, MgB_2, which adopts an AlB_2-type structure with boron honeycomb layers alternating with Mg metallic sheets, is the highest-temperature conventional superconductor known at atmospheric pressure with a T_c of 39 K.[5] This (relatively) high T_c has, over the years, favored numerous studies aiming to optimize MgB_2 superconducting characteristics (chemical doping) and/or to discover novel related boron-containing compounds.[18] More recently, superconductivity was also observed in the new ternary layered compound $Sc_{20}BC_{27}$ at T_c = 7.7 K.[8] Using Eliashberg

theory,[19] the experimentally characterized three-dimensional clathrate SrB_3C_3[20] was predicted to be a high-temperature conventional superconductor with T_c up to ∼40 K at ambient pressure,[21] and recent experiments indicate superconductivity above 20 K under pressure.[9] Higher T_cs were recently predicted for related hypothetical binary-guest C−B clathrates.[22,23]

Superconductivity was also experimentally demonstrated for some layered MB_2C_2 (M = rare-earth metal) compounds, such as YB_2C_2 or LuB_2C_2 with T_c = 3.6 and 2.4 K, respectively.[24,25] Higher T_cs have been predicted for some hypothetical MB_2C_2 compounds containing alkali and alkaline-earth metals.[7,26,27] Using Eliashberg theory and the Allen–Dynes formula,[28,29] one of us has speculated that T_cs higher than that reported for MgB_2 could also be observed for some structurally related layered alkali-metal $M_{0.5}BC_2$ (M = Li, Na, and K) compounds.[30] Comparable T_cs have been proposed for MgB_2-like Li_xBC ($x < 1.0$),[6] $Li_4B_5C_3$, and Li_2B_3C.[31] An analysis of the electronic structure of $M_{0.5}BC_2$ reveals that the DOS at the Fermi energy is strongly B–C σ-bonding in character. It was demonstrated that the σ character is indeed essential for reaching high T_c values because the B–C σ-bonding states couple strongly with the bending-like phonon modes of the BC_2 layers. With these results in mind, though they have not been proved yet experimentally, we thought that it would be worth extending the study carried out on $M_{0.5}BC_2$ to some existing and hypothetical rare-earth metal or alkaline-earth metal MB_2C_2-layered compounds to explore their possible superconductivity using first-principles electron–phonon calculations.

Structures of rare-earth-metal and alkaline-earth-metal MB_2C_2 (M = Sc, Y, Be, Ca) layered compounds, which are part of ternary solid-state rare-earth metal boride carbides,[32–34] consist of the stacking of alternatively two-dimensional (2D) B/C layers and metal sheets (Figure 1). Depending on the metal, different B/C topologies are experimentally encountered. For instance, fused 4- and 8-membered rings (48^2 network) are observed in YB_2C_2[35–38] and CaB_2C_2,[39] fused 5- and 7-membered rings (57^2 network) appear in ScB_2C_2,[40,41] and fused 6-membered rings (6^3 network) are found in BeB_2C_2,[42] the latter being somewhat related to MgB_2C_2.[43] High or moderate T_c superconductivity has been achieved or predicted for compounds with 6^3 honeycomb networks. Therefore, it is of great interest to investigate whether high-T_c superconductivity can also emerge in layered compounds with networks other than 6^3. As mentioned above, high-T_c superconductivity is essentially related to the B–C σ-bonding of sp^2 hybridized orbitals. In the structures of the 48^2 and 57^2 networks, B–C bonding angles somewhat deviate from the ideal 120° angle of sp^2 bonding. In this situation, deviation from true sp^2 hybridization may significantly affect the energy levels and strength of the σ-bonding, and consequently T_c. For this reason, we theoretically investigated existing or hypothetical MB_2C_2-layered structures to examine the occurrence of superconductivity and the dependence of T_c with respect to their structural, vibrational, and electronic properties.

2. CALCULATION METHODS

Calculations of the electronic structures were conducted using the Quantum ESPRESSO (QE) code[44,45] based on density functional theory (DFT) with plane waves and pseudopotentials. The ultrasoft pseudopotentials[46] of boron, carbon, and metal atoms were used from the library of QE.[47] The generalized gradient approximation functional of Perdew, Burke, and Ernzerhof was employed.[48] An energy cutoff of 50 Ry for plane waves and 350 Ry for electron density was sufficient to provide convergence of the total energy. The total energies were calculated upon optimization of the lattice parameters and the atomic positions of the experimentally confirmed structures taking into account the boron/carbon distribution (B vs C coloring problem) (see Figure 1),[33,37,39,41] using a Monkhorst–Pack *k*-point sampling,[49] with an (8 × 4 × 8) mesh for ScB_2C_2 and (8 × 8 × 8) meshes for BeB_2C_2, YB_2C_2, and CaB_2C_2. For the substituted phases of BeB_2C_2 and CaB_2C_2, the structures were optimized starting from the same initial structures as the nonsubstituted phases with M being replaced, using the same meshes as those used for the nondoped phases. Their optimized structures are provided in Figure S1 and Table S1 in the Supporting Information. The convergence threshold for the forces on atoms was 10^{-4} a.u.

Phonon dispersion curves and Eliashberg spectral functions (α^2F) were calculated by using the PHonon code available in the QE package. For the calculation of electron–phonon coupling coefficients, fine meshes of (24 × 24 × 24) to (48 × 48 × 48) were used for the Fermi surface calculations. The *k*-grid and *q*-grid meshes for ScB_2C_2 were (8 × 4 × 8) and (4 × 2 × 4), respectively. For BeB_2C_2, YB_2C_2, and CaB_2C_2, both meshes were (4 × 4 × 4). The summation at the Fermi energy was performed using the interpolation method.[50] Using the Fermi surface data, the optimal broadening parameters were determined to maximize the integration of the DOS at the Fermi level, ensuring the most accurate summation of electron–phonon interaction calculations. T_c values were estimated using the Allen–Dynes formula,[28,29] with a Coulomb repulsion parameter μ^* of 0.1. For a convergence test concerning the *k*- and *q*-grid meshes in electron-phonon interaction calculations, we compared (8 × 8 × 8) and (4 × 4 × 4) *k*-grid meshes for YB_2C_2 and observed an error in T_c of 0.1 K. The (4 × 4 × 4) and (2 × 2 × 2) *q*-grid meshes for YB_2C_2 produced a difference in T_c of 0.01 K.

3. RESULTS AND DISCUSSION

3.1. Electronic Structures. The DOS at the Fermi level, phonon dispersion curves, and Eliashberg spectral functions are necessary to elucidate whether superconductivity can be achieved. The electronic DOS was first calculated and analyzed for each of the unsubstituted rare-earth-

metal and alkaline-earth metal ScB_2C_2, YB_2C_2, BeB_2C_2, and CaB_2C_2 compounds (Figure 2). It has been proposed previously that the electronic properties of a boron–carbon network – and therefore the electrical properties of the $M_xB_yC_z$ compounds – are related to the average valence electron concentration (VEC) per main group atom.[51] Assuming a Zintl–Klemm ionic bonding scheme between the metal and the nonmetal atoms in a first approximation, VEC is given by VEC = $(nx + 3y + 4z)/(y + z)$, where n is the number of valence electrons of the metal. This was checked with theoretical studies, which have shown that MB_2C_2 compounds having a VEC of 4 should display semiconducting properties,[33,42] whereas those with more (or less) than 4 should be metallic in character. This is confirmed again here (Figure 2), where MB_2C_2 compounds are metallic with the trivalent Sc and Y metals (VEC = 4.25) and semiconducting with the divalent Be and Ca metals (VEC = 4.0) with narrow band gaps of approximately 0.3 eV (insets in Figure 2c,d).

3.2. Superconductivity. The calculated DOS (Figure 2) suggests that ScB_2C_2 and YB_2C_2 could potentially exhibit superconductivity, while BeB_2C_2 and CaB_2C_2 may not unless carrier doping is applied. It is generally admitted that the necessary condition for a metallic compound to become a superconductor is the simultaneous occurrence of flat and steep bands reflected in high peaks of DOS at the Fermi level with a fairly large coupling of the flat band states with the lattice phonons.[52,53] The electronic band structures of the compounds listed in Table 1 are provided in the Supporting Information (Figure S2). Overall, these band structures appear to feature both flat and steep bands around the Fermi level. T_cs for these materials were calculated and are listed in Table 1, which were then analyzed for each case of metal M.

3.2.1. Case of ScB_2C_2 and YB_2C_2. ScB_2C_2 and YB_2C_2, which contain trivalent metals, are expected to exhibit superconductivity, regardless of the topology of the boron–carbon layer structure: 57^2 network for ScB_2C_2 and 48^2 network for YB_2C_2 (see Figure 1). The calculated T_cs are weak, 0.5 and 4.7 K for ScB_2C_2 and YB_2C_2, respectively. Interestingly, the computed T_c for YB_2C_2 is close to the experimental value, as reported by Sakai et al. (3.6 K)[24] and Michor et al. (1.0 K).[25] The reason for their relatively low T_cs compared with MgB_2[5] and doped MBC[6,7,27] was examined from the partial DOS of the constituent atoms. Figures 3 and 4 show the total and atomic orbital-projected DOS of ScB_2C_2 and YB_2C_2, respectively. For the former, there are two distinct positions for B and C atoms. "B with B" indicates B atoms adjacent to other B atoms, while "B with C" refers to B atoms with only C neighbors (Figure 1a). The same notation applies to C atoms. It is observed that the electronic states at the Fermi level (0 eV) predominantly consist of p_z orbitals (red lines) of the B and C atoms, along with d orbitals of the Sc atoms. The p_z orbitals of B and C

atoms are geometrically perpendicular to the B_2C_2 planes and exhibit a small π overlap with each other.

This situation is demonstrated in Figure 5a, which shows the spatial distributions of the local DOS at the Fermi level projected onto planes perpendicular to the B_2C_2 planes. Here, the local DOS at the Fermi level indicates the contributions to the electron density distribution from the crystal orbitals near the Fermi energy. It is clearly observed that p_z-like electrons at the Fermi level are localized on B and C atoms, and d-like electrons are similarly localized on Sc atoms. Under these circumstances, the electronic states at the Fermi level are minimally influenced by atomic oscillations, leading to relatively weak electron–phonon interactions (Eliashberg function), as depicted in Figure 6a. The values of the Eliashberg function of ScB_2C_2 are much smaller than those of hole-doped BeB_2C_2, for instance, which will be presented in the next section.

The preceding discussion also thoroughly applies to YB_2C_2, with its atomic orbital-projected DOS, spatial distribution of local DOS at the Fermi level, and Eliashberg function as shown in Figures 4, 5b, and 6b, respectively. The slightly higher T_c computed for YB_2C_2 compared to ScB_2C_2 may result from the higher Debye frequency of YB_2C_2 (1328 cm^{-1}) compared to that of ScB_2C_2 (1205 cm^{-1}). The experimental value of the T_c for YB_2C_2 (3.6[24] or 1.0 K[25]) is slightly lower than the calculated value (4.7 K). This difference might be explained by structural disturbances in experimental samples, as argued in the case of hole-doped LiBC.[54–56] However, since the calculation of T_c inevitably includes some error, we do not delve into further detail.

3.2.2. Case of BeB_2C_2 (6^3 network). As said earlier, BeB_2C_2 exhibits semiconductive behavior (Figure 2c) and cannot be superconductive. We therefore attempted (heavy) carrier doping by substituting some Be atoms with Li (hole doping) or Al (electron doping). One Be atom out of four in the unit cell was replaced by a Li or an Al atom to produce $Li_{0.25}Be_{0.75}B_2C_2$ (VEC = 3.94) and $Al_{0.25}Be_{0.75}B_2C_2$ (VEC = 4.06). These two compositions were computed to be thermodynamically stable and exhibited no imaginary phonon modes. Their kinetic stabilities were also confirmed by Parrinello–Rahman MD simulations (Figure S3 in the Supporting Information). Interestingly, the T_c calculated for $Li_{0.25}Be_{0.75}B_2C_2$, 47.8 K (Table 1), is high and is comparable to that reported experimentally for MgB_2[5] and those predicted T_cs for hole-doped LiBC and MgB_2C_2.[6,7] The electronic structure of $Li_{0.25}Be_{0.75}B_2C_2$ is shown in Figure 7. The total DOS (Figure 7a) exhibits the features of hole-doping, and the orbital-projected DOS of B and C (Figure 7b,c) indicate that the peak of DOS at the Fermi level mainly consists of bonding σ-states made of p_x (green line) and p_y (dashed blue line) components with almost no p_z (red line) participation. The atomic orbital-

projected DOS of Be and Li are almost null at the Fermi level (they are omitted in the figure). This indicates that electrons at the Fermi level extend parallel to the B_2C_2 plane.

Figure 8 displays the spatial distributions of the local DOS at the Fermi level projected onto planes perpendicular to the BC planes. In $Li_{0.25}Be_{0.75}B_2C_2$ (Figure 8a), it is observed that the electrons at the Fermi level are distributed between the B and C atoms. Because of this, the electronic states at the Fermi level are significantly influenced by atomic oscillations, leading to relatively strong electron–phonon interactions, as shown in Figure 9a, contrasting with the cases of the trivalent-metal-containing ScB_2C_2 and YB_2C_2 presented in the previous section (Figures 5 and 6). The value of the Eliashberg function is particularly high in the range between 800 and 1000 cm^{-1} (Figure 9a) corresponding to the bending modes of phonons (Figure 9c), where the bond angles mainly change.

Regarding the hole doping of BeB_2C_2, Moudden[27] removed 1/3 of the Be atoms ($Be_{2/3}B_2C_2$) and evaluated T_c at 31 K (Table 1). Although the resulting T_c falls within the same range as in our study, the phonon spectrum suggested structural instability.[27] In this case, the number of holes (or removed electrons), 0.67 per chemical formula, is much larger than 0.25 in our case ($Li_{0.25}Be_{0.75}B_2C_2$). We attempted further substitution of Be with Li by producing $Li_{0.5}Be_{0.5}B_2C_2$; however, the structure generated slightly imaginary phonon modes. It is uncertain whether these are intrinsic or due to technical issues.

In contrast to the (heavy) hole-doped case ($Li_{0.25}Be_{0.75}B_2C_2$), a lower T_c of 5.1 K is computed for electron-doped $Al_{0.25}Be_{0.75}B_2C_2$ (Table 1). Its electronic structure is depicted in Figure 7. The atomic orbital-projected DOS of B and C (Figure 7e,f) demonstrate that the DOS at the Fermi level consists almost entirely of p_z (red line) orbitals. The spatial distribution of the DOS at the Fermi level is depicted in Figure 8b. This distribution is rather similar to those of the trivalent metal cases ScB_2C_2 and YB_2C_2, as shown in Figure 5. Consequently, it is understandable that the electron–phonon interaction in $Al_{0.25}Be_{0.75}B_2C_2$ (Figure 9b) is as weak as that in ScB_2C_2 and YB_2C_2 (Figure 6), resulting in a low T_c.

3.2.3. Case of CaB_2C_2 (48^2 network). As mentioned earlier, CaB_2C_2 with a 48^2 network (Figure 1d) exhibits semiconductive behavior similar to BeB_2C_2 (Figure 2c,d). We attempted both (heavy) hole and electron doping by substituting 1/4 of Ca with K and Sc, respectively. The kinetic stabilities of the doped compounds were confirmed through Parrinello–Rahman MD simulations (Figure S3 in the Supporting Information). As a result, hole-doped $K_{0.25}Ca_{0.75}B_2C_2$ shows a low computed T_c of 3.1 K (Table 1), which unexpectedly contrasts with the high T_c (47.8 K) of the hole-doped $Li_{0.25}Be_{0.75}B_2C_2$ compound.

The reason for this was examined from its electronic structure (Figure 10). The electronic states at the Fermi level mostly consist of π-states made of p_z orbitals (red lines) of B and C atoms (Figure 10b,c). Therefore, the situation here is rather similar to that in the electron-carrier systems ScB_2C_2, YB_2C_2 (Figure 4), and $Al_{0.25}Be_{0.75}B_2C_2$ (Figures 7d–f). In $K_{0.25}Ca_{0.75}B_2C_2$, the spatial distribution of the states at the Fermi-level is localized in turn on atoms (Figure 11a), which is similar to the above-mentioned electron-carrier systems (Figures 5 and 8b), except that electrons are more localized on C atoms. By the same mechanism as that of the electron-carrier systems, $K_{0.25}Ca_{0.75}B_2C_2$ exhibits weak electron–phonon interactions (Figure 12a), leading to the low T_c. Thus, although CaB_2C_2 and BeB_2C_2 have a divalent metal atom in common, superconductivity appears in a different manner upon hole doping due to the different layer structures of BC.

Electron-doped $Sc_{0.25}Ca_{0.75}B_2C_2$ also exhibits a low computed T_c value of 1.9 K (Table 1). Similar to those of the hole-doped $K_{0.25}Ca_{0.75}B_2C_2$ compound, the electronic states at the Fermi level mostly consist of p_z orbitals of the B and C atoms (Figure 10d–f), which is consistent with other electron-carrier systems mentioned above. In $Sc_{0.25}Ca_{0.75}B_2C_2$, the spatial distribution of the states at the Fermi level is strongly localized on B and C atoms (Figure 11b), where p_z orbitals of B predominate over those of C. For the same reasons observed in the electron-carrier systems, the electron–phonon interactions are weak (Figure 12b), resulting in a low T_c. In summary, for CaB_2C_2, both hole and electron doping yield low T_cs, which contrasts with the case of BeB_2C_2.

4. CONCLUSIONS

In this work, the possible superconductivity of the several layered metal boride carbide MB_2C_2 was theoretically studied. Results show that all of them could be superconductors with T_cs, strongly influenced by both the topology of the boron–carbon layers and the valence of the metal atoms. With trivalent metals, ScB_2C_2 and YB_2C_2 exhibit superconductivity with low computed T_cs, regardless of the boron–carbon 2D arrangements: 57^2 network (ScB_2C_2) or 48^2 network (YB_2C_2). These predicted low T_cs are in agreement with experiments, which showed that YB_2C_2 is a superconductor at very low temperatures. With divalent metals, BeB_2C_2 and CaB_2C_2 become superconductive upon (heavy) carrier doping, but superconductivity emerges differently depending on the topology of the boron–carbon sheets. Interestingly, for BeB_2C_2 with a 6^3 network, hole doping ($Li_{0.25}Be_{0.75}B_2C_2$) results in a high T_c (47.8 K), while electron doping ($Al_{0.25}Be_{0.75}B_2C_2$) leads to a low T_c. In contrast, for CaB_2C_2, with a 48^2 network, both hole doping ($K_{0.25}Ca_{0.75}B_2C_2$) and electron doping ($Sc_{0.25}Ca_{0.75}B_2C_2$) result in low T_cs. The difference in T_c originates from the spatial distribution of the electronic states at the Fermi level. In cases of low T_c (ScB_2C_2, YB_2C_2, e- or h-doped CaB_2C_2, and e-doped BeB_2C_2), electrons at the Fermi level are

localized in π states predominantly made of B and C p_z-orbital components perpendicular to the BC layers. Therefore, the electronic states at the Fermi level are less affected by atomic oscillations, leading to weak electron–phonon interactions. On the other hand, in the case of high T_c (h-doped BeB_2C_2), electrons at the Fermi level reside in σ states in the region between B and C atoms and are significantly affected by atomic oscillations, resulting in strong electron–phonon interactions.

Results discussed in this paper seem to indicate that electron-poor (h-doped) metal boride carbide MB_2C_2 compounds with a 6^3 boron–carbon network could be promising superconductor candidates with T_cs comparable or superior to those of MgB_2, which also contains 6^3 honeycomb planes. These theoretical findings should strongly encourage further experimental works in this direction.

ASSOCIATED CONTENT

Supporting Information

The Supporting Information is available free of charge at https://pubs.acs.org/doi/10.1021/acs.inorgchem.4c02221.

ACKNOWLEDGMENTS

The calculations in this study were conducted using the Numerical Materials Simulator at NIMS.

REFERENCES

(1) Drozdov, A. P.; Eremets, M. I.; Troyan, I. A.; Ksenofontov, V.; Shylin, S. I. Conventional superconductivity at 203 Kelvin at high pressures in the sulfur hydride system. *Nature* **2015**, *525*, 73–76.

(2) Somayazulu, M.; Ahart, M.; Mishra, A. K.; Geballe, Z. M.; Baldini, M.; Meng, Y.; Struzhkin, V. V.; Hemley, R. J. Evidence for Superconductivity above 260 K in Lanthanum Superhydride at Megabar Pressures. *Phys. Rev. Lett.* **2019,** *122*, 027001.

(3) Drozdov, A. P.; Kong, P. P.; Minkov, V. S.; Besedin, S. P.; Kuzovnikov, M. A.; Mozaffari, S.; Balicas, L.; Balakirev, F. F.; Graf, D. E.; Prakapenka, V. B.; Greenberg, E.; Knyazev, D. A.; Tkacz, M.; Eremets, M. I. Superconductivity at 250 K in lanthanum hydride under high pressures. *Nature* **2019**, *569*, 528–531.

(4) Boeri, L.; Hennig, R.; Hirschfeld, P.; Profeta, G.; Sanna, A.; Zurek, E.; Pickett, W. E.; Amsler, M.; Dias, R.; Eremets, M. I.; Heil, C.; Hemley, R. J.; Liu, H.; Ma, Y.; Pierleoni, C.; Kolmogorov, A. N.; Rybin, N.; Novoselov, D.; Anisimov, V.; Oganov, A. R.; Pickard, C. J.; Bi, T.; Arita, R.; Errea, I.; Pellegrini, C.; Requist, R.; Gross, E. K. U.;

Margine, E. R.; Xie, S. R.; Quan, Y.; Hire, A.; Fanfarillo, L.; Stewart, G. R.; Hamlin, J. J.; Stanev, V.; Gonnelli, R. S.; Piatti, E.; Romanin, D.; Daghero, D.; Valenti, R. The 2021 room-temperature superconductivity roadmap. *J. Phys. Condens. Matter* **2022**, *34*, 183002.

(5) Nagamatsu, J.; Nakagawa, N.; Muranaka, T.; Zenitani, Y.; Akimitsu, J. Superconductivity at 39 K in magnesium diboride. *Nature* **2001**, *410*, 63–64.

(6) Rosner, H.; Kitaigorodsky, A.; Pickett, W. E. Prediction of high T_c superconductivity in hole-doped LiBC. *Phys. Rev. Lett.* **2002**, *88*, 127001.

(7) Verma, A. K.; Modak, P.; Gaitonde, D. M.; Rao, R. S.; Godwal, B. K.; Gupta, L. C. Possible high-temperature superconductivity in hole-doped MgB_2C_2. *Europhys. Lett.* **2003**, *63*, 743–749.

(8) Ninomiya, H.; Oka, K.; Hase, I.; Kawashima, K.; Fujihisa, H.; Gotoh, Y.; Ishida, S.; Ogino, H.; Iyo, A.; Yoshida, Y.; Eisaki, H. Superconductivity in a scandium borocarbide with a layered crystal structure. *Inorg. Chem.* **2019**, *58*, 15629–15636.

(9) Zhu, L.; Liu, H.; Somayazulu, M.; Meng, Y.; Guńka, P. A.; Shiell, T. B.; Kenney-Benson, C.; Chariton, S.; Prakapenka, V. B.; Yoon, H.; Horn, J. A.; Paglione, J.; Hoffmann, R.; Cohen, R. E.; Strobel, T. A. Superconductivity in SrB_3C_3 clathrate. *Phys. Rev. Res.* **2023**, *5*, 013012.

(10) Chen, S.; Wu, Z.; Zhang, Z.; Wu, S.; Ho, K. M.; Antropov, V.; Sun, Y. High-throughput screening for boride superconductors. *Inorg. Chem.* **2024**, *63*, 8654–8663.

(11) (a) Cava, R. J.; Takagi, T.; Batlogg, B.; Zandbergen, H. W.; Krajewski, J. J.; Peck, Jr., W. F.; van Dover, R. B.; Felder, R. J.; Siegrist, T.; Mizuhashi, K.; Lee, J. O.; Eisaki, H.; Carter, S. A.; Uchida, S. Superconductivity at 23 K in yttrium palladium boride carbide. *Nature*, **1994**, *367*, 146–148. (b) R. J. Cava, R. J.; Takagi, H.; Zandbergen, H. W.; Krajewski, J. J.; Peck, Jr., W. F.; Siegrist, T.; Batlogg, B.; van Dover, R. B.; Felder, R. J.; Mizuhashi, K.; Lee, J. O.; Eisaki, H.; Uchida, S. Superconductivity in the quaternary intermetallic compounds $LnNi_2B_2C$. *Nature* **1994**, *367*, 252–253.

(12) Nagarajan, R. Mazumdar, C.; Hossain, Z.; Dhar, S. K.; Golpakrishnan, K. V.; Gupta, L. C.; Godart, C.; Padalia, B. D.; Vijayaraghavan, R. Bulk superconductivity at an elevated temperature (T 12 K) in a nickel containing alloy system Y-Ni-B-C. *Phys. Rev. Lett.* **1994**, *72*, 274–277.

(13) Sarrao, J. L.; de Andrade, M. C.; Herrmann, J.; Han, S. H.; Fisk, Z.; Maple, M. B.; Cava, R. J. Superconductivity to 21 K in intermetallic thorium-based boride carbides. *Physica C* **1994**, *229*, 65–69.

(14) Pickett, W. E.; Singh, D. J. $LuNi_2B_2C$: A novel Ni-based strong-coupling superconductor *Phys. Rev. Lett.* **1994**, *72*, 3702–3705.

(15) Burdett, J. K.; Sevov, S. Electronic Structure of the $RENi_2B_2C$ Superconductor. *Inorg.Chem.* **1994**, *33*, 3857–3858.

(16) Halet, J.-F. Electronic Structure of the Superconducting Rare-Earth-Metal Nickel Boron Carbide Compounds. *Inorg. Chem.* **1994**, *33*, 4173–4178.

(17) Singh, D. J.; Electronic Properties of YNi_2B_2C. Solid State Commun. **1996**, *98*, 899–902.

(18) Muralidhar, M.; Shadab, M.; Sai Srikanth, A.; Jirsa, M.; Noudem, J. Review on high-performance bulk MgB_2 superconductors. *J. Phys. D: Appl. Phys.* **2023**, *57*, 053001.

(19) Marsiglio, F. Eliashberg theory: A short review. *Ann. Phys.* **2020**, *417*, 168102.

(20) Zhu, L.; Borstad, G. M.; Liu, H.; Guńka, P. A.; Guerette, M.; Dolyniuk, J.-A.; Meng, Y.; Greenberg, E.; Prakapenka, V. B.; Chaloux, B. L.; Epshteyn, A.; Cohen, R. E.; Strobel, T. A. Carbon-boron clathrates as a new class of sp^3-bonded framework materials. *Sci. Adv.* **2020**, *6*, eaay8361.

(21) Wang, J.-N.; Yan, X.-W.; Gao, M. High-temperature superconductivity in SrB_3C_3 and BaB_3C_3 predicted from first-principles anisotropic Migdal-Eliashberg theory. *Phys. Rev. B* **2021**, *103*, 144515.

(22) Di Cataldo, S.; Qulaghasi, S.; Bachelet, G. B.; Boeri, L. High-T_c superconductivity in doped boron-carbon clathrates. *Phys. Rev. B* **2022**, *105*, 064516.

(23) Geng, N.; Hilleke, K. P.; Zhu, L.; Wang, X.; Strobel, T. A.; Zurek, E. Conventional High-Temperature Superconductivity in Metallic, Covalently Bonded, Binary-Guest C-B Clathrates. *J. Am. Chem. Soc.* **2023**, *145*, 1696–1706.

(24) Sakai, T.; Adachi, G.-Y.; Shiokawa, J. Electrical Properties of Rare Earth Diborodicarbides (RB_2C_2-Type Layer Compounds). *J. Less-Common Met.* **1982**, *84*, 107–114.

(25) Michor, H.; Scheidt, E. W.; Manalo, S.; Müller, M.; Bauer, E.; Hilscher, G. Superconductivity in layered YB_2C_2. *J. Phys.: Conf. Ser.* **2009**, *150*, 052160.

(26) Spanò, E.; Bernasconi, M.; Kopnin, E., Electron-phonon interaction in hole-doped MgB_2C_2. *Phys. Rev. B* **2005**, *72*, 014530.

(27) Moudden, A. H. Strong electron-phonon coupling in $Be_{1-x}B_2C_2$: ab initio studies. *Eur. Phys. J. B* **2008**, *64*, 173–183.

(28) McMillan, W. L. Transition Temperature of Strong-Coupled Superconductors. *Phys. Rev.* **1968**, *167*, 331–344.

(29) Allen, P. B.; Dynes, R. C. Transition temperature of strong-coupled superconductors reanalyzed. *Phys. Rev. B* **1975**, *12*, 905–922.

(30) Hayami, W.; Tanaka, T., Superconductivity of alkali-metal intercalated BC_2. *AIP Adv.* **2020**, *10*, 065213.

(31) Bazhirov, T.; Sakai, Y.; Saito, S.; Cohen, M. L. Electron-phonon coupling and superconductivity in Li-intercalated layered borocarbide compounds. *Phys. Rev. B* **2014**, *89*, 045136.

(32) Bauer, J.; Halet, J.-F.; Saillard, J.-Y. Rare earth metal borocarbides: Examples of coordination compounds in solid-state chemistry. *Coord. Chem. Rev.* **1998**, *178–180*, 723–753.

(33) Rocquefelte, X.; Boulfelfel, S. E.; Ben Yahia, M.; Bauer, J.; Saillard, J.-Y.; Halet, J.-F. Structural preference versus metal within the MB_2C_2 (M = Mg, Sc, Ca, Y, Ln) phases: the coloring problem revisited by DFT calculations. *Angew. Chem. Int. Ed.* **2005**, *44*, 7542–7545.

(34) Babizhetskyy, V.; Bauer, J.; Gautier, R.; Hiebl, K.; Simon, A.; Halet, J.-F. Structural, Electronic, and Physical Properties of Solid-State Rare-Earth Boride Carbides. In *Handbook on the Physics and Chemistry of Rare Earths including Actinides*, Bünzli, J.-C.; Pecharsky, V. K., Eds. North-Holland: **2018**, Vol. 53, pp 145–269.

(35) Smith, P. K.; Gilles, P. W. High temperature rare earth-boron-carbon studies—III LnB_2C_2 and the ternary phase diagram. *J. Inorg. Nucl. Chem.* **1967**, *29*, 375–382.

(36) Bauer, J.; Nowotny, H. The ternary system yttrium-boron-carbon. *Monatsh. Chem.* **1971**, *102*, 1129–1145.

(37) Khmelevskyi, S.; Mohn, P.; Redinger, J.; Michor, H. Electronic structure of the layered diboride dicarbide superconductor YB_2C_2. *Supercond. Sci. Technol.* **2005**, *18*, 422–426.

(38) Reckeweg, O.; DiSalvo, F. J. Different structural models of YB_2C_2 and GdB_2C_2 on the basis of single-crystal X-ray data. *Naturforsch. B* **2014**, *69* (3), 289–293.

(39) Albert, B.; Schmitt, K. CaB_2C_2: Reinvestigation of a semiconducting boride carbide with a layered structure and an interesting boron/carbon ordering scheme. *Inorg. Chem.* **1999**, *38*, 6159–6163.

(40) Smith, G. S.; Johnson, Q.; Nordine, P. C., The crystal structure of ScB_2C_2. *Acta Crystallogr.* **1965**, *19*, 668–673.

(41) Lassoued, S.; Boucher, B.; Boutarfaia, A.; Gautier, R.; Halet, J.-F. The coloring problem in the solid-state metal boride carbide ScB_2C_2: a theoretical analysis. *Z. Naturforsch. B* **2016**, *71*, 593–601.

(42) Hofmann, K.; Rocquefelte, X.; Halet, J.-F.; Bahtz, C.; Albert, B. The η^6,η^1-coordination of beryllium atoms in the graphite analogue BeB_2C_2. *Angew. Chem. Int. Ed.* **2008**, *47*, 2301–2303.

(43) Wörle, M.; Nesper, R. MgB_2C_2, a new graphite-related refractory compound. *J. Alloys Compd.* **1994**, *216*, 75–83.

(44) Giannozzi, P.; Baroni, S.; Bonini, N.; Calandra, M.; Car, R.; Cavazzoni, C.; Ceresoli, D.; Chiarotti, G. L.; Cococcioni, M.; Dabo, I.; Dal Corso, A.; de Gironcoli, S.; Fabris, S.; Fratesi, G.; Gebauer, R.; Gerstmann, U.; Gougoussis, C.; Kokalj, A.; Lazzeri, M.; Martin-Samos, L.; Marzari, N.; Mauri, F.; Mazzarello, R.; Paolini, S.; Pasquarello, A.; Paulatto, L.; Sbraccia, C.; Scandolo, S.; Sclauzero, G.; Seitsonen, A. P.; Smogunov, A.; Umari, P.; Wentzcovitch, R. M. QUANTUM ESPRESSO: a modular and open-source software project for quantum simulations of materials. *J. Phys.: Condens. Matter* **2009**, *21*, 395502.

(45) Giannozzi, P.; Andreussi, O.; Brumme, T.; Bunau, O.; Buongiorno Nardelli, M.; Calandra, M.; Car, R.; Cavazzoni, C.; Ceresoli, D.; Cococcioni, M.; Colonna, N.; Carnimeo, I.; Dal Corso, A.; de Gironcoli, S.; Delugas, P.; DiStasio, R. A.; Ferretti, A.; Floris, A.; Fratesi, G.; Fugallo, G.; Gebauer, R.; Gerstmann, U.; Giustino, F.; Gorni, T.; Jia, J.; Kawamura, M.; Ko, H. Y.; Kokalj, A.; Küçükbenli, E.; Lazzeri, M.; Marsili, M.; Marzari, N.; Mauri, F.; Nguyen, N. L.; Nguyen, H. V.; Otero-de-la-Roza, A.; Paulatto, L.; Poncé, S.; Rocca, D.; Sabatini, R.; Santra, B.; Schlipf, M.; Seitsonen, A. P.; Smogunov, A.; Timrov, I.; Thonhauser, T.; Umari, P.; Vast, N.; Wu, X.; Baroni, S. Advanced capabilities for materials modelling with Quantum ESPRESSO. *J. Phys.: Condens. Matter* **2017**, *29*, 465901.

(46) Vanderbilt, D. Soft self-consistent pseudopotentials in a generalized eigenvalue formalism. *Phys. Rev. B* **1990**, *41*, 7892–7895.

(47) Quantum ESPRESSO, http://www.quantum-espresso.org.

(48) Perdew, J. P.; Burke, K.; Ernzerhof, M. Generalized Gradient Approximation Made Simple. *Phys. Rev. Lett.* **1996**, *77*, 3865–3868.

(49) Monkhorst, H. J.; Pack, J. D. Special points for Brillouin-zone integrations. *Phys. Rev. B* **1976**, *13*, 5188–5192.

(50) Wierzbowska, M.; de Gironcoli, S.; Giannozzi, P. Origins of low- and high-pressure discontinuities of T_c in niobium. *arXiv:cond-mat/0504077v2* **2006**.

(51) Wiitkar, F.; Kahlal, S.; Halet, J.-F.; Saillard, J.-Y.; Bauer, J.; Rogl, P. Electronic structure of layered MB_2C rare-earth borocarbide compounds. *J. Am. Chem. Soc*. **1994**, *116*, 251–261.

(52) Simon, A. Superconductivity and the periodic table: from elements to materials. *Phil. Trans. R. Soc. A* **2015**, *373*, 20140192.

(53) Yang, Z. S.; Ferrenti, A. M.; Cava, R. J. Testing whether flat bands in the calculated electronic density of states are good predictors of superconducting materials. *J. Phys. Chem. Solids* **2021**, *151*, 109912.

(54) Fogg, A. M.; Chalker, P. R.; Claridge, J. B.; Darling, G. R.; Rosseinsky, M. J. LiBC electronic, vibrational, structural, and low-temperature chemical behavior of a layered material isoelectronic with MgB_2. *Phys. Rev. B* **2003**, *67*, 245106.

(55) Souptel, D.; Hossain, Z.; Behr, G.; Löser, W.; Geibel, C. Synthesis and physical properties of LiBC intermetallics. *Solid State Commun.* **2003**, *125*, 17–21.

(56) Nakamori, Y.; Orimo, S.-i. Synthesis and characterization of single phase Li_xBC (x=0.5 and 1.0), using Li hydride as a starting material. *J. Alloys and Compd*. **2004**, *370*, L7–L9.

Table 1. Calculated T_cs, Vertex Symbols of 2D Network, VEC, and Carrier Types of Unsubstituted and Partially Substituted MB_2C_2 (M = Sc, Y, Be, Ca). Carrier Type: electron (e) or hole (h)

compound	T_c (K)	2D network	VEC	carrier type	remarks
ScB_2C_2	0.5	57^2	4.25	e	
YB_2C_2	4.7	48^2	4.25	e	exp. 3.6 K,[24] 1.0 K[25]
BeB_2C_2		6^3	4.0		semiconductor
$Li_{0.25}Be_{0.75}B_2C_2$	47.8	6^3	3.94	h	
$Al_{0.25}Be_{0.75}B_2C_2$	5.1	6^3	4.06	e	
$Be_{2/3}B_2C_2$	31	6^3	3.83	h	ref. 27
CaB_2C_2		48^2	4.0		semiconductor
$K_{0.25}Ca_{0.75}B_2C_2$	3.5	48^2	3.94	h	
$Sc_{0.25}Ca_{0.75}B_2C_2$	1.9	48^2	4.06	e	

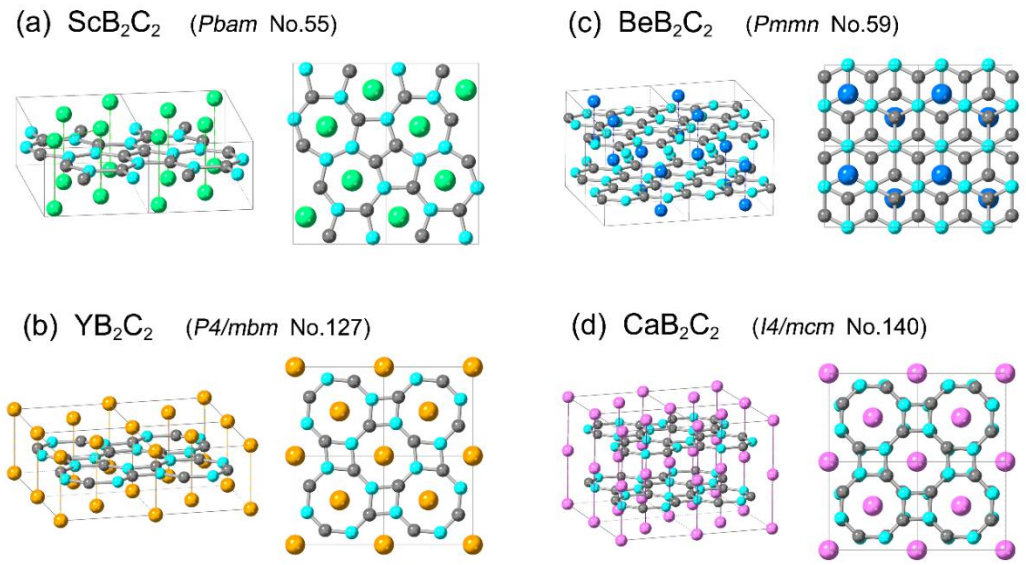

Figure 1. Side and top views of MB_2C_2 structures (M = Sc (a), Y (b), Be (c), and Ca (d)). Small spheres represent boron (light blue) and carbon (gray) atoms. Larger spheres (green, orange, blue, and pink) represent metal atoms.

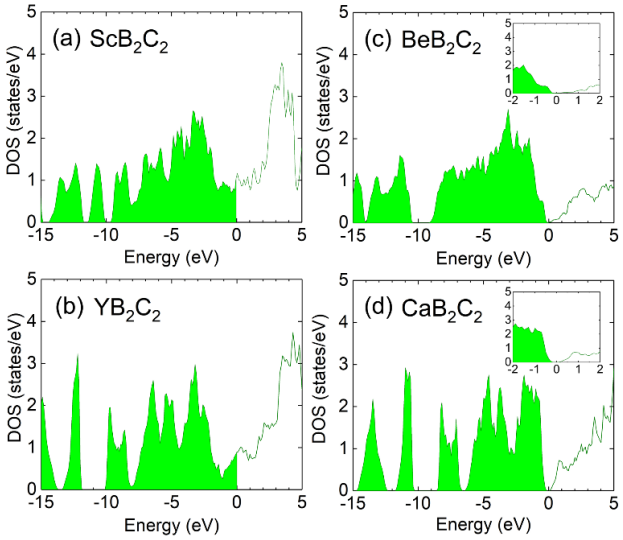

Figure 2. Electronic DOS per chemical formula for MB_2C_2 (M = Sc (a), Y(b), Be (c), and Ca (d)). The Fermi level is defined as zero. Insets in parts (c) and (d) show the DOS enlarged around the Fermi level.

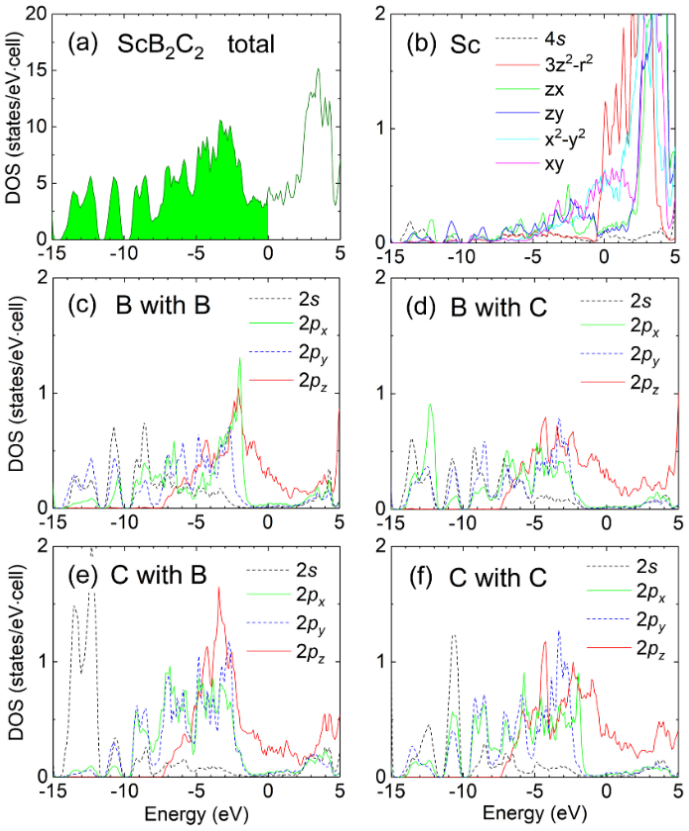

Figure 3. Total (a) and atomic orbital-projected (b–f) DOS for ScB_2C_2. "B with B" in panel (c) refers to boron atoms adjacent to other B atoms, while "B with C" in panel (d) refers to boron atoms with only C neighbors (see Figure 1a). The same notation applies to "C with B" and "C with C". The Fermi level is set at 0. Crystal axes are chosen in such a way that the *z* axis is perpendicular to the B_2C_2 layers.

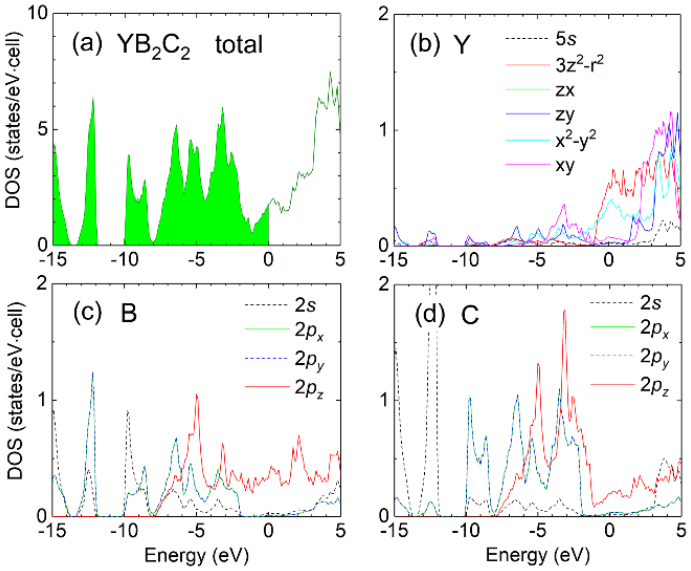

Figure 4. Total (a) and atomic orbital-projected (b–d) DOS for YB_2C_2. The Fermi level is set at 0.

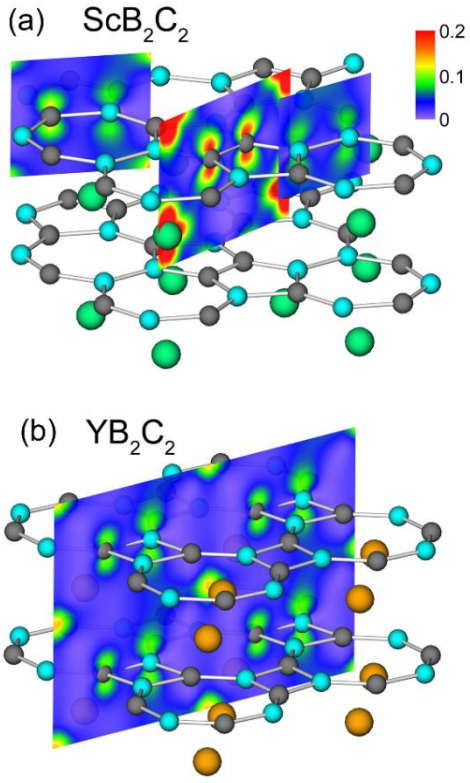

Figure 5. Spatial distributions of the local DOS at the Fermi level projected onto planes perpendicular to the B_2C_2 planes for ScB_2C_2 (a) and YB_2C_2 (b). Small spheres represent B (light blue) and C (gray) atoms, while large spheres represent Sc (green) and Y (orange) atoms, respectively. The color scale unit is states/(bohr^3 Ry).

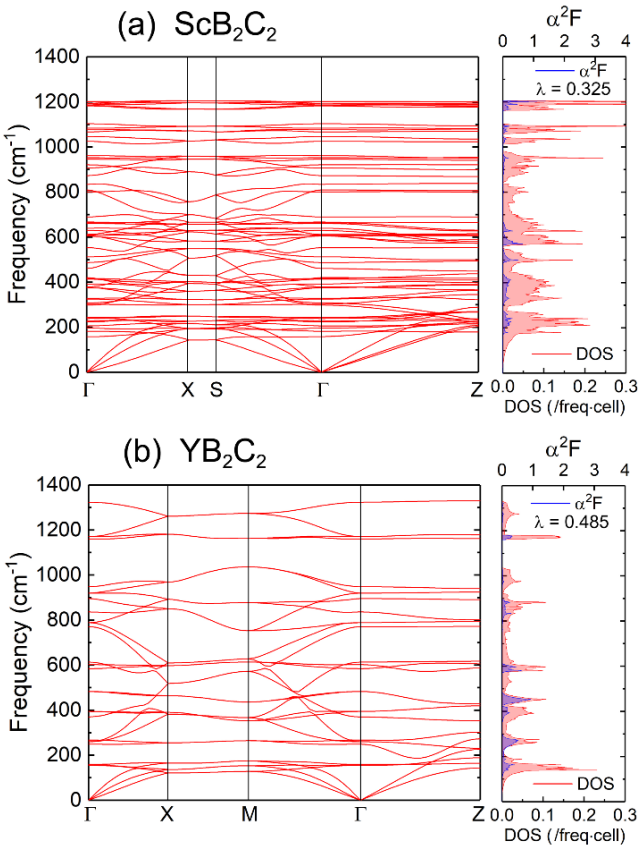

Figure 6. Phonon dispersion curves (left) with DOS and Eliashberg function α^2F (right) for (a) ScB_2C_2 and (b) YB_2C_2. The values of λ in the right graph are electron–phonon coupling constants.

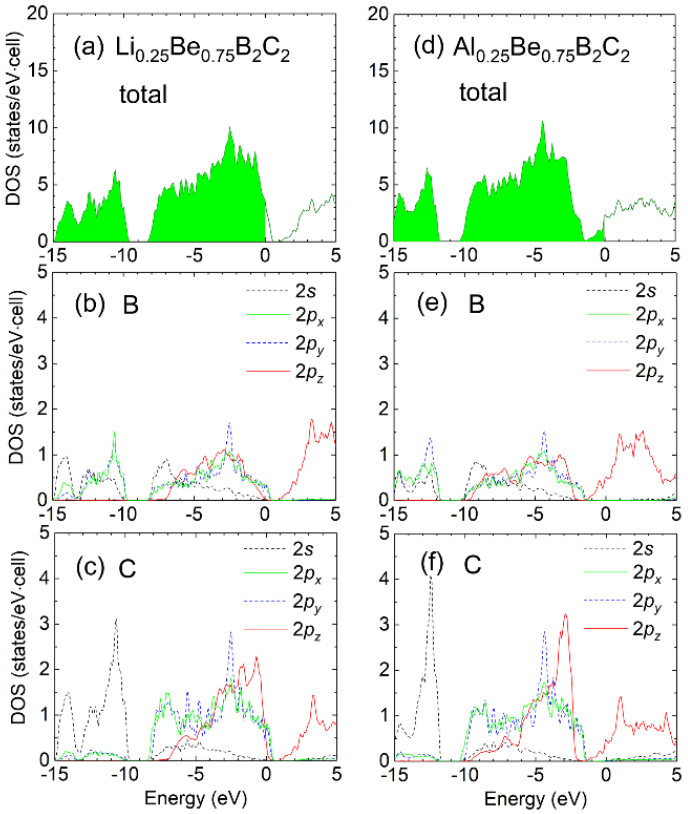

Figure 7. Total and atomic orbital-projected DOS for $Li_{0.25}Be_{0.75}B_2C_2$ (a–c) and $Al_{0.25}Be_{0.75}B_2C_2$ (d–f). The Fermi level is set at 0. The *z* axis is perpendicular to the B_2C_2 layers.

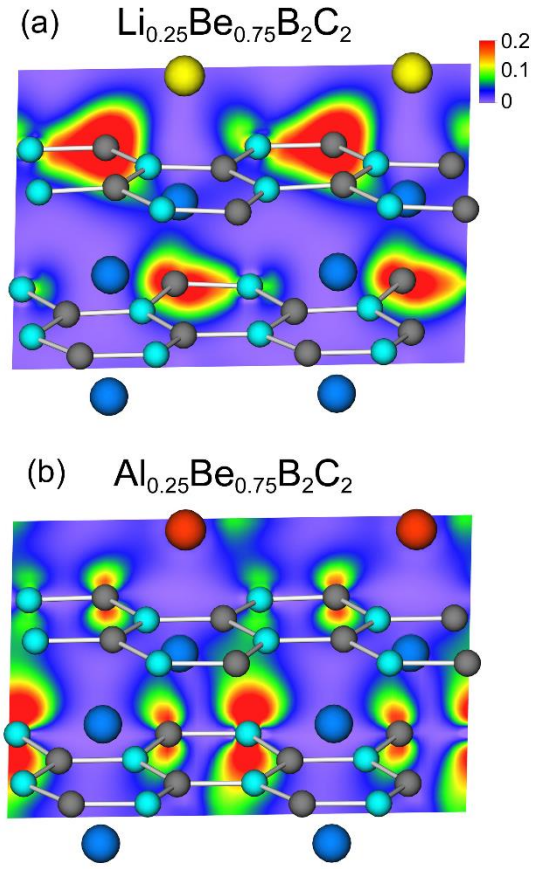

Figure 8. Spatial distributions of the local DOS at the Fermi level projected onto planes perpendicular to the B_2C_2 planes for $Li_{0.25}Be_{0.75}B_2C_2$ (a) and $Al_{0.25}Be_{0.75}B_2C_2$ (b). Small spheres represent B (light blue) and C (gray) atoms, while large spheres represent Be (blue), Li (yellow), and Al (red) atoms. The color scale unit is states/(bohr^3 Ry).

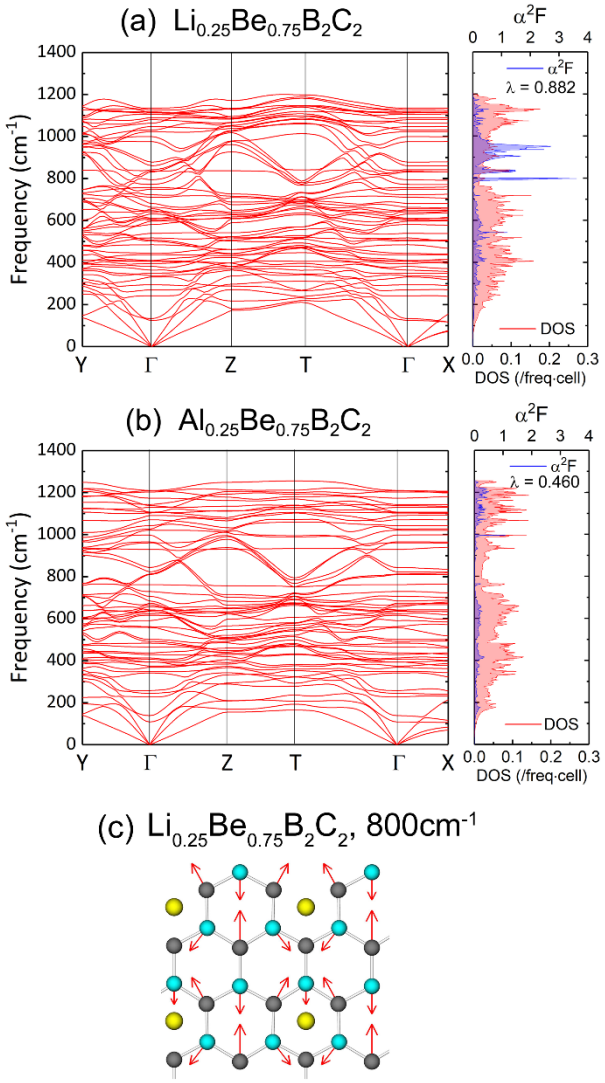

Figure 9. Phonon dispersion curves (left) with DOS and the Eliashberg function α^2F (right) for (a) $Li_{0.25}Be_{0.75}B_2C_2$ and (b) $Al_{0.25}Be_{0.75}B_2C_2$. (c) Vibration vector corresponding to the highest peak of α^2F at 800 cm^{-1} in panel (a). The values of λ in the right graph are electron–phonon coupling constants.

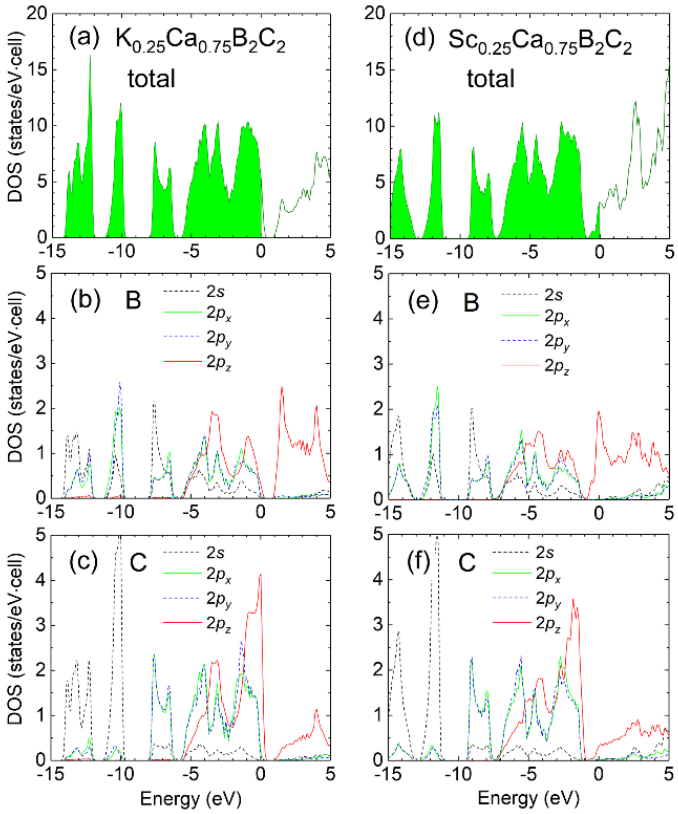

Figure 10. Total and atomic orbital-projected DOS for $K_{0.25}Ca_{0.75}B_2C_2$ (a–c) and $Sc_{0.25}Ca_{0.75}B_2C_2$ (d–f). The Fermi level is set at 0.

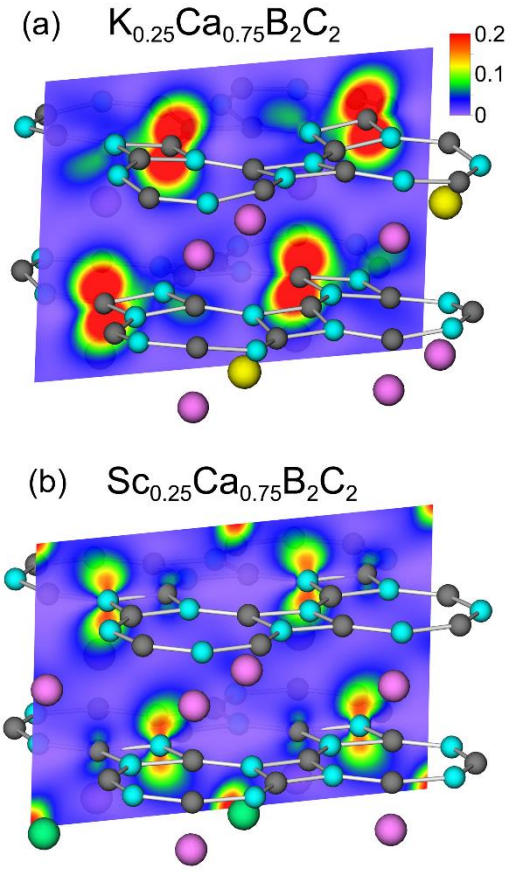

Figure 11. Spatial distributions of the local DOS at the Fermi level projected onto planes perpendicular to the B_2C_2 planes for $K_{0.25}Ca_{0.75}B_2C_2$ (a) and $Sc_{0.25}Ca_{0.75}B_2C_2$ (b). Small spheres represent B (light blue) and C (gray) atoms, and large spheres represent Ca (pink), K (yellow), and Sc (green) atoms. The unit of the color scale is states/(bohr^3 Ry).

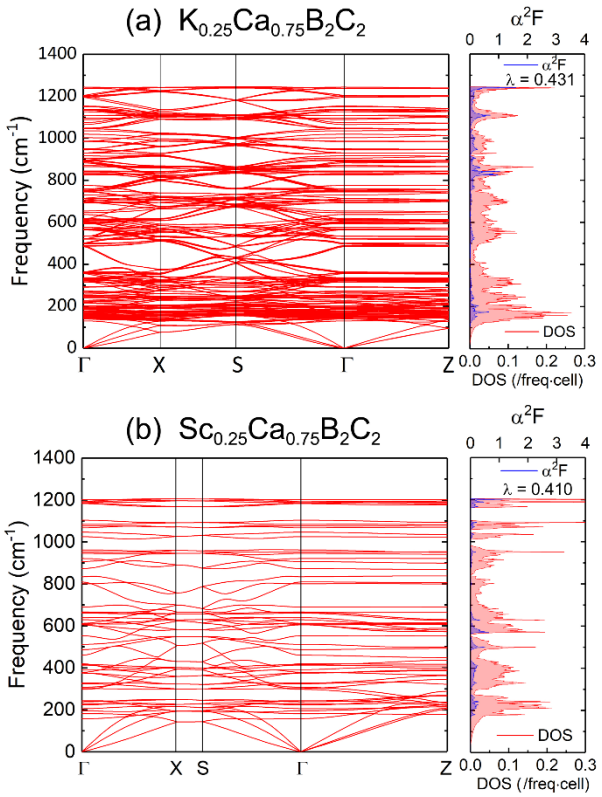

Figure 12. Phonon dispersion curves (left) with DOS and the Eliashberg function α^2F (right) for (a) $K_{0.25}Ca_{0.75}B_2C_2$ and (b) $Sc_{0.25}Ca_{0.75}B_2C_2$. The values of λ in the right graph are electron–phonon coupling constants.

Supporting Information

Possible Superconductivity for Layered Metal Boride Carbide Compounds MB_2C_2 (M = Alkali, Alkaline-Earth or Rare-Earth Metals)

Wataru Hayami,[1*] Xavier Rocquefelte,[2] and Jean-François Halet[2,3]*

[1]*Research Center for Materials Nanoarchitectonics, National Institute for Materials Science, Namiki 1-1, Tsukuba, Ibaraki 305-0044, Japan*

[2]*Univ Rennes, CNRS, Ecole Nationale Supérieure de Chimie de Rennes (ENSCR), Institut des Sciences Chimiques de Rennes (ISCR), UMR 6226, F-35000 Rennes, France*

[3]*CNRS–Saint-Gobain–NIMS, IRL 3629, Laboratory for Innovative Key Materials and Structures (LINK), National Institute for Materials Science (NIMS), Tsukuba 305-0044, Japan*

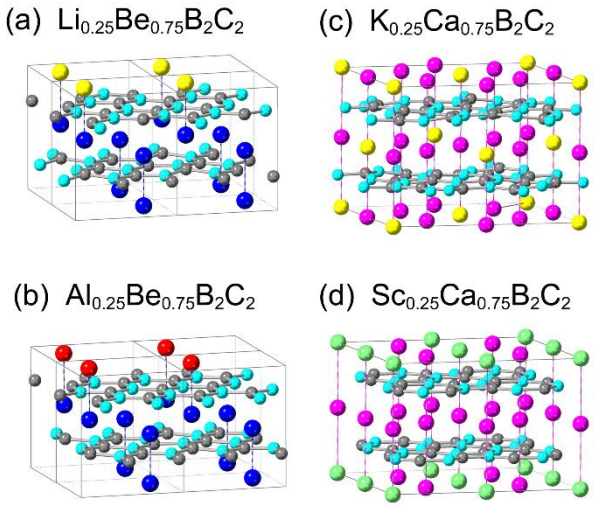

Figure S1. Optimized structures of the doped phases $Li_{0.25}Be_{0.75}B_2C_2$ (a) and $Al_{0.25}Be_{0.75}B_2C_2$ (b) derived from BeB_2C_2, and $K_{0.25}Ca_{0.75}B_2C_2$ (c) and $Sc_{0.25}Ca_{0.75}B_2C_2$ (d) derived from CaB_2C_2. One Be (blue) out of four is replaced by Li (yellow) in (a), and Al (red) in (b). One Ca (pink) out of four is replaced by K (yellow) in (c), and Sc (green) in (d). B and C are represented by light blue and grey spheres, respectively.

* Corresponding authors. E-mail: hayami.wataru@nims.go.jp (W.H.), Jean-Francois.Halet@univ-rennes.fr (J.-F. H.)

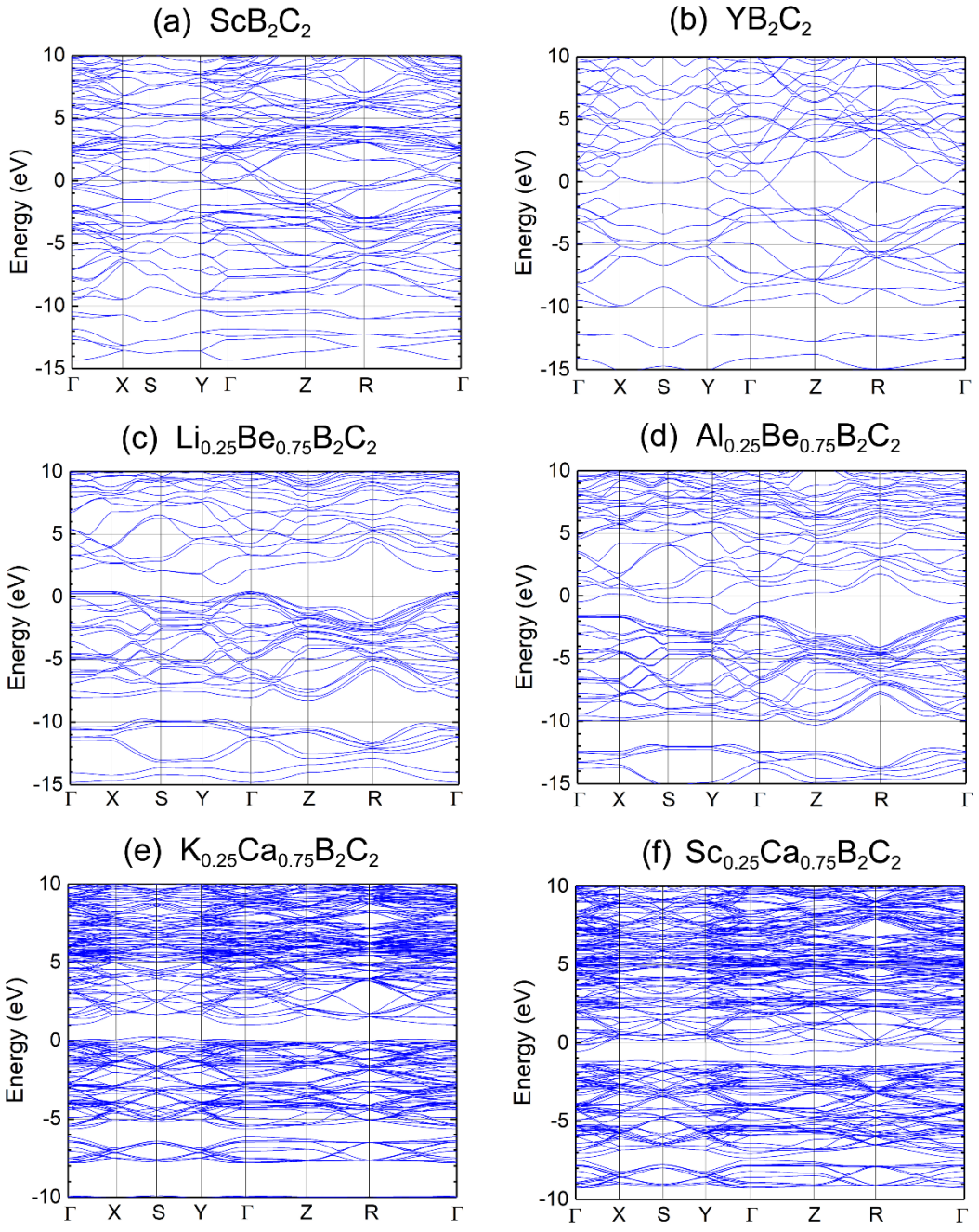

Figure S2. Electronic band structures of ScB_2C_2 (a), YB_2C_2 (b), $Li_{0.25}Be_{0.75}B_2C_2$ (c), $Al_{0.25}Be_{0.75}B_2C_2$ (d), $K_{0.25}Ca_{0.75}B_2C_2$ (e), and $Sc_{0.25}Ca_{0.75}B_2C_2$ (f).

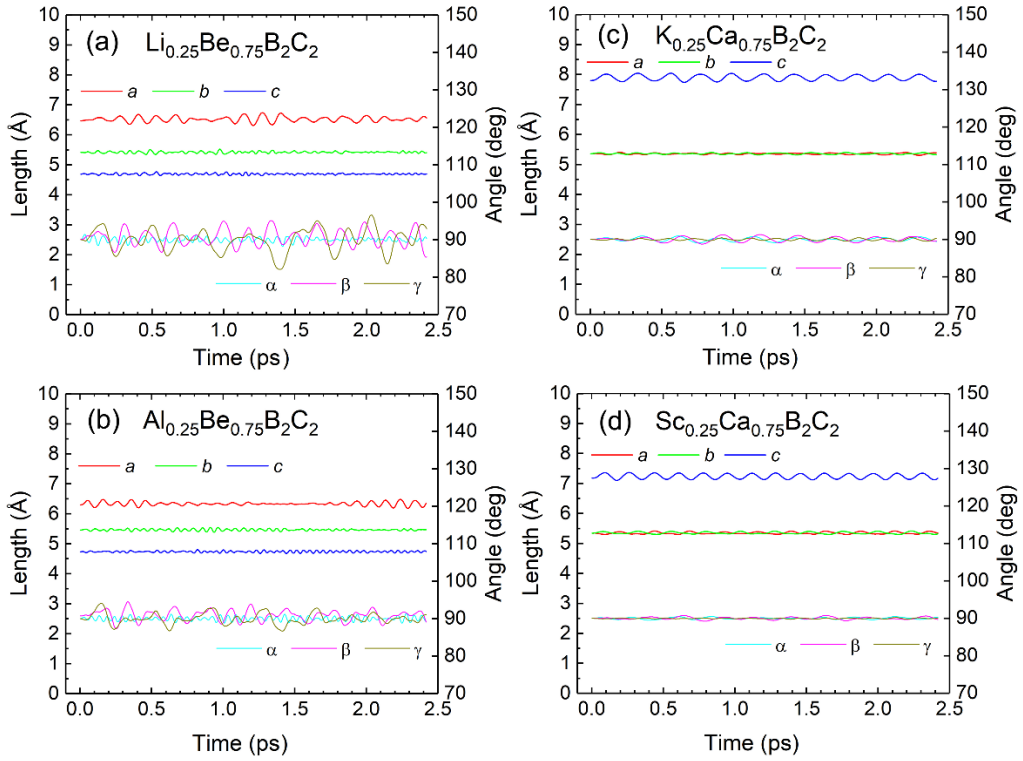

Figure S3. Fluctuations of the lattice parameters of the doped phases $Li_{0.25}Be_{0.75}B_2C_2$ (a) and $Al_{0.25}Be_{0.75}B_2C_2$ (b) derived from BeB_2C_2, and $K_{0.25}Ca_{0.75}B_2C_2$ (c) and $Sc_{0.25}Ca_{0.75}B_2C_2$ (d) derived from CaB_2C_2, during Parrinello-Rahman MD simulations performed at 300 K, 1 atm. (*a*, *b*, *c*) are the lattice lengths, and (α, β, γ) are the lattice angles. The atomic coordinates were nearly identical between the initial and final steps (see Figure S1).

Table S1. Optimized lattice parameters and fractional atomic coordinates.

Optimized lattice paremeters.

compounds	*a* (Å)	*b* (Å)	*c* (Å)	α (deg)	β (deg)	γ (deg)
ScB_2C_2	5.2811	10.1977	3.4435	90.0	90.0	90.0
YB_2C_2	5.3505	5.3505	3.5796	90.0	90.0	90.0
BeB_2C_2	6.1341	5.4328	4.6997	90.0	90.0	90.0
$Li_{0.25}Be_{0.75}B_2C_2$	6.4643	5.4141	4.6845	90.0	90.1	90.0
$Al_{0.25}Be_{0.75}B_2C_2$	6.2964	5.4579	4.7289	90.0	90.7	90.0
CaB_2C_2	5.3624	5.3624	7.4160	90.0	90.0	90.0
$K_{0.25}Ca_{0.75}B_2C_2$	5.3579	5.3579	7.7971	90.0	90.0	90.0
$Sc_{0.25}Ca_{0.75}B_2C_2$	5.3406	5.3406	7.1759	90.0	90.0	90.0

Optimized fractional atomic coordinates.

ScB_2C_2

Sc	0.1378487640	0.1485379615	0.0000000000
Sc	0.8621512360	0.8514620385	0.0000000000
Sc	0.3621512360	0.6485379615	0.0000000000
Sc	0.6378487640	0.3514620385	0.0000000000
B	0.3560234215	0.4644938330	0.5000000000
B	0.6439765785	0.5355061670	0.5000000000
B	0.1439765785	0.9644938330	0.5000000000
B	0.8560234215	0.0355061670	0.5000000000
B	0.9867208808	0.3110484420	0.5000000000
B	0.0132791192	0.6889515580	0.5000000000
B	0.5132791192	0.8110484420	0.5000000000
B	0.4867208808	0.1889515580	0.5000000000
C	0.3928050638	0.0445390380	0.5000000000
C	0.6071949362	0.9554609620	0.5000000000
C	0.1071949362	0.5445390380	0.5000000000
C	0.8928050638	0.4554609620	0.5000000000
C	0.2968104770	0.3092045552	0.5000000000
C	0.7031895230	0.6907954448	0.5000000000
C	0.2031895230	0.8092045552	0.5000000000
C	0.7968104770	0.1907954448	0.5000000000

YB_2C_2

Y	0.0000000000	0.0000000000	0.0000000000
Y	0.5000000000	0.5000000000	0.0000000000
B	0.1367863516	0.3632136484	0.5000000000
B	0.8632136484	0.6367863516	0.5000000000
B	0.6367863516	0.1367863516	0.5000000000

B	0.3632136484	0.8632136484	0.5000000000
C	0.1618245098	0.6618245098	0.5000000000
C	0.8381754902	0.3381754902	0.5000000000
C	0.3381754902	0.1618245098	0.5000000000
C	0.6618245098	0.8381754902	0.5000000000

BeB_2C_2

Be	0.0467917894	0.7500000000	0.3172291807
Be	0.4532082106	0.7500000000	0.3172291807
Be	0.5467917894	0.2500000000	0.6827708193
Be	0.9532082106	0.2500000000	0.6827708193
B	0.2500000000	0.0018011523	0.4918737008
B	0.2500000000	0.2500000000	0.0007886657
B	0.2500000000	0.4981988477	0.4918737008
B	0.2500000000	0.7500000000	-0.0213206621
B	0.7500000000	-0.0018011523	0.5081262992
B	0.7500000000	0.2500000000	0.0213206621
B	0.7500000000	0.5018011523	0.5081262992
B	0.7500000000	0.7500000000	-0.0007886657
C	0.2500000000	-0.0069118397	0.1602987924
C	0.2500000000	0.2500000000	0.6659522374
C	0.2500000000	0.5069118397	0.1602987924
C	0.2500000000	0.7500000000	0.6445049778
C	0.7500000000	0.0069118397	0.8397012076
C	0.7500000000	0.2500000000	0.3554950222
C	0.7500000000	0.4930881603	0.8397012076
C	0.7500000000	0.7500000000	0.3340477626

$Li_{0.25}Be_{0.75}B_2C_2$

Be	0.0466972312	0.7500000000	0.3234977152
Be	0.4540856362	0.7500000000	0.3179915708
Be	0.5533358051	0.2500000000	0.6782558781
Li	0.9734371936	0.2500000000	0.6899956019
B	0.2586807430	0.0039176942	0.4934045279
B	0.2659065611	0.2500000000	-0.0038284409
B	0.2586807430	0.4960823058	0.4934045279
B	0.2501865565	0.7500000000	-0.0192475999
B	0.7431142823	-0.0013194231	0.5070953978
B	0.7337430441	0.2500000000	0.0190071616
B	0.7431142823	0.5013194231	0.5070953978
B	0.7344988148	0.7500000000	-0.0033439418
C	0.2538801932	-0.0066684966	0.1608972541
C	0.2786352783	0.2500000000	0.6665334650
C	0.2538801932	0.5066684966	0.1608972541
C	0.2494816825	0.7500000000	0.6450667945
C	0.7325660757	0.0044697191	0.8395152358
C	0.7368163147	0.2500000000	0.3509149785
C	0.7325660757	0.4955302809	0.8395152358
C	0.7466932937	0.7500000000	0.3333319858

$Al_{0.25}Be_{0.75}B_2C_2$

Be	0.0452665437	0.7500000000	0.3084351211
Be	0.4552788478	0.7500000000	0.3070150463
Be	0.5465414894	0.2500000000	0.6915745424
Al	0.9693550621	0.2500000000	0.7079075482
B	0.2580866153	-0.0004007542	0.4786659214
B	0.2698508763	0.2500000000	-0.0038328323
B	0.2580866153	0.5004007542	0.4786659214
B	0.2523066995	0.7500000000	-0.0311667290
B	0.7382847116	-0.0047939283	0.5154571369
B	0.7306212546	0.2500000000	0.0348531169
B	0.7382847116	0.5047939283	0.5154571369
B	0.7411356664	0.7500000000	0.0077139399
C	0.2554681384	-0.0061865776	0.1486390830
C	0.2697482643	0.2500000000	0.6515202918
C	0.2554681384	0.5061865776	0.1486390830
C	0.2507260303	0.7500000000	0.6336839798
C	0.7401598220	0.0033763399	0.8498105792
C	0.7391509237	0.2500000000	0.3643027402
C	0.7401598220	0.4966236601	0.8498105792
C	0.7460197672	0.7500000000	0.3428477937

CaB_2C_2

Ca	0.5000000000	0.5000000000	0.7499997358
Ca	0.0000000000	0.0000000000	0.2500001756
Ca	0.0000000000	0.0000000000	0.7499998244
Ca	0.5000000000	0.5000000000	0.2500002642
B	0.1388374252	0.3611625818	0.5000000000
B	0.8611625748	0.6388374182	0.5000000000
B	0.6388374182	0.1388374252	0.5000000000
B	0.3611625818	0.8611625748	0.5000000000
B	0.8611626428	0.3611626178	0.0000000000
B	0.1388373572	0.6388373822	0.0000000000
B	0.3611626178	0.1388373572	0.0000000000
B	0.6388373822	0.8611626428	0.0000000000
C	0.6594060003	0.8405939834	0.5000000000
C	0.3405939997	0.1594060166	0.5000000000
C	0.1594060166	0.6594060003	0.5000000000
C	0.8405939834	0.3405939997	0.5000000000
C	0.8405939627	0.6594060640	0.0000000000
C	0.6594060640	0.1594060373	0.0000000000
C	0.1594060373	0.3405939360	0.0000000000
C	0.3405939360	0.8405939627	0.0000000000

$K_{0.25}Ca_{0.75}B_2C_2$ * (2 × 2 × 1) unit cell of CaB_2C_2

Ca	0.2499699370	0.2499703159	0.7500094619
K	0.0000000000	0.0000000000	0.2499963687

Ca	0.0000000000	0.0000000000	0.7500188534
Ca	0.2499680555	0.2499680614	0.2499911291
B	0.0699839732	0.1806567115	0.5083653007
B	0.4298987569	0.3192827382	0.5083543149
B	0.3192991406	0.0699902099	0.4916335312
B	0.1806673913	0.4299153102	0.4916405014
B	0.4299160117	0.1806672481	0.0083569301
B	0.0699895160	0.3192990849	0.0083646391
B	0.1806574067	0.0699835579	-0.0083611279
B	0.3192826217	0.4298994429	-0.0083544737
C	0.3280054515	0.4200707842	0.5152173688
C	0.1719481898	0.0799622057	0.5152270721
C	0.0799561878	0.3279966049	0.4847876300
C	0.4200590754	0.1719345985	0.4847598386
C	0.4200702648	0.3280056234	-0.0152179615
C	0.3279969138	0.0799561793	0.0152117516
C	0.0799626115	0.1719478980	-0.0152242454
C	0.1719338426	0.4200588143	0.0152377619
Ca	0.7500296841	0.2499699370	0.7500094619
Ca	0.5000000000	-0.0000000000	0.2499903259
K	0.5000000000	-0.0000000000	0.7500038093
Ca	0.7500319386	0.2499680555	0.2499911291
B	0.5700846898	0.1806673913	0.4916405014
B	0.9300097901	0.3192991406	0.4916335312
B	0.8193432885	0.0699839732	0.5083653007
B	0.6807172618	0.4298987569	0.5083543149
B	0.9300164421	0.1806574067	-0.0083611279
B	0.5701005571	0.3192826217	-0.0083544737
B	0.6807009151	0.0699895160	0.0083646391
B	0.8193327519	0.4299160117	0.0083569301
C	0.8280654015	0.4200590754	0.4847598386
C	0.6720033951	0.0799561878	0.4847876300
C	0.5799292158	0.3280054515	0.5152173688
C	0.9200377943	0.1719481898	0.5152270721
C	0.9200438207	0.3279969138	0.0152117516
C	0.8280521020	0.0799626115	-0.0152242454
C	0.5799411857	0.1719338426	0.0152377619
C	0.6719943766	0.4200702648	-0.0152179615
Ca	0.2499703159	0.7500300630	0.7500094619
Ca	0.0000000000	0.5000000000	0.2499903259
K	0.0000000000	0.5000000000	0.7500038093
Ca	0.2499680614	0.7500319445	0.2499911291
B	0.0699902099	0.6807008594	0.4916335312
B	0.4299153102	0.8193326087	0.4916405014
B	0.3192827382	0.5701012431	0.5083543149
B	0.1806567115	0.9300160268	0.5083653007
B	0.4298994429	0.6807173783	-0.0083544737
B	0.0699835579	0.8193425933	-0.0083611279
B	0.1806672481	0.5700839883	0.0083569301
B	0.3192990849	0.9300104840	0.0083646391
C	0.3279966049	0.9200438122	0.4847876300

C	0.1719345985	0.5799409246	0.4847598386
C	0.0799622057	0.8280518102	0.5152270721
C	0.4200707842	0.6719945485	0.5152173688
C	0.4200588143	0.8280661574	0.0152377619
C	0.3280056234	0.5799297352	-0.0152179615
C	0.0799561793	0.6720030862	0.0152117516
C	0.1719478980	0.9200373885	-0.0152242454
Ca	0.7500300630	0.7500296841	0.7500094619
K	0.5000000000	0.5000000000	0.2499939424
Ca	0.5000000000	0.5000000000	0.7500048738
Ca	0.7500319445	0.7500319386	0.2499911291
B	0.5701012431	0.6807172618	0.5083543149
B	0.9300160268	0.8193432885	0.5083653007
B	0.8193326087	0.5700846898	0.4916405014
B	0.6807008594	0.9300097901	0.4916335312
B	0.9300104840	0.6807009151	0.0083646391
B	0.5700839883	0.8193327519	0.0083569301
B	0.6807173783	0.5701005571	-0.0083544737
B	0.8193425933	0.9300164421	-0.0083611279
C	0.8280518102	0.9200377943	0.5152270721
C	0.6719945485	0.5799292158	0.5152173688
C	0.5799409246	0.8280654015	0.4847598386
C	0.9200438122	0.6720033951	0.4847876300
C	0.9200373885	0.8280521020	-0.0152242454
C	0.8280661574	0.5799411857	0.0152377619
C	0.5799297352	0.6719943766	-0.0152179615
C	0.6720030862	0.9200438207	0.0152117516

$Sc_{0.25}Ca_{0.75}B_2C_2$ * (2 × 2 × 1) unit cell of CaB_2C_2

Ca	0.2499860229	0.2499859895	0.7499998933
Sc	0.0000000000	0.0000000000	0.2500010303
Ca	0.0000000000	0.0000000000	0.7500006933
Ca	0.2499821331	0.2499822246	0.2499998611
B	0.0685249716	0.1805627236	0.4883943168
B	0.4314016973	0.3193499622	0.4884006677
B	0.3193417502	0.0685148072	0.4883991993
B	0.1805661271	0.4314278729	0.4883960053
B	0.4314278777	0.1805661263	0.0116039535
B	0.0685147767	0.3193417431	0.0116006460
B	0.1805627001	0.0685249673	0.0116057475
B	0.3193499369	0.4314017070	0.0115991938
C	0.3311364988	0.4203846351	0.4876491099
C	0.1687951213	0.0796019657	0.4876400197
C	0.0796172877	0.3311280342	0.4876539348
C	0.4203675975	0.1687809923	0.4876423832
C	0.4203846572	0.3311364720	0.0123507776
C	0.3311279734	0.0796172904	0.0123458485
C	0.0796019364	0.1687951636	0.0123599333
C	0.1687810023	0.4203676228	0.0123574320
Ca	0.7500140105	0.2499860229	0.7499998933

Sc	0.5000000000	-0.0000000000	0.2500006702
Ca	0.5000000000	-0.0000000000	0.7500004975
Ca	0.7500177754	0.2499821331	0.2499998611
B	0.5685721271	0.1805661271	0.4883960053
B	0.9314851928	0.3193417502	0.4883991993
B	0.8194372764	0.0685249716	0.4883943168
B	0.6806500378	0.4314016973	0.4884006677
B	0.9314750327	0.1805627001	0.0116057475
B	0.5685982930	0.3193499369	0.0115991938
B	0.6806582569	0.0685147767	0.0116006460
B	0.8194338737	0.4314278777	0.0116039535
C	0.8312190077	0.4203675975	0.4876423832
C	0.6688719658	0.0796172877	0.4876539348
C	0.5796153649	0.3311364988	0.4876491099
C	0.9203980343	0.1687951213	0.4876400197
C	0.9203827096	0.3311279734	0.0123458485
C	0.8312048364	0.0796019364	0.0123599333
C	0.5796323772	0.1687810023	0.0123574320
C	0.6688635280	0.4203846572	0.0123507776
Ca	0.2499859895	0.7500139771	0.7499998933
Sc	0.0000000000	0.5000000000	0.2500006702
Ca	0.0000000000	0.5000000000	0.7500004975
Ca	0.2499822246	0.7500178669	0.2499998611
B	0.0685148072	0.6806582498	0.4883991993
B	0.4314278729	0.8194338729	0.4883960053
B	0.3193499622	0.5685983027	0.4884006677
B	0.1805627236	0.9314750284	0.4883943168
B	0.4314017070	0.6806500631	0.0115991938
B	0.0685249673	0.8194372999	0.0116057475
B	0.1805661263	0.5685721223	0.0116039535
B	0.3193417431	0.9314852233	0.0116006460
C	0.3311280342	0.9203827123	0.4876539348
C	0.1687809923	0.5796324025	0.4876423832
C	0.0796019657	0.8312048787	0.4876400197
C	0.4203846351	0.6688635012	0.4876491099
C	0.4203676228	0.8312189977	0.0123574320
C	0.3311364720	0.5796153428	0.0123507776
C	0.0796172904	0.6688720266	0.0123458485
C	0.1687951636	0.9203980636	0.0123599333
Ca	0.7500139771	0.7500140105	0.7499998933
Sc	0.5000000000	0.5000000000	0.2500000814
Ca	0.5000000000	0.5000000000	0.7500001660
Ca	0.7500178669	0.7500177754	0.2499998611
B	0.5685983027	0.6806500378	0.4884006677
B	0.9314750284	0.8194372764	0.4883943168
B	0.8194338729	0.5685721271	0.4883960053
B	0.6806582498	0.9314851928	0.4883991993
B	0.9314852233	0.6806582569	0.0116006460
B	0.5685721223	0.8194338737	0.0116039535
B	0.6806500631	0.5685982930	0.0115991938
B	0.8194372999	0.9314750327	0.0116057475

C	0.8312048787	0.9203980343	0.4876400197
C	0.6688635012	0.5796153649	0.4876491099
C	0.5796324025	0.8312190077	0.4876423832
C	0.9203827123	0.6688719658	0.4876539348
C	0.9203980636	0.8312048364	0.0123599333
C	0.8312189977	0.5796323772	0.0123574320
C	0.5796153428	0.6688635280	0.0123507776
C	0.6688720266	0.9203827096	0.0123458485